Journal of Alloys and Compounds 695 (2017) 520–525

Contents lists available at ScienceDirect

Journal of Alloys and Compounds

journal homepage: http://www.elsevier.com/locate/jalcom

High performance humidity sensor based on metal organic framework MIL-101(Cr) nanoparticles

Jingjing Zhang [a], Liang Sun [c], Chuan Chen [c], Man Liu [a], Wei Dong [a], Wenbin Guo [a, **], Shengping Ruan [a, b, *]

[a] State Key Laboratory on Integrated Optoelectronics, College of Electronic Science & Engineering, Jilin University, Changchun 130012, PR China
[b] State Key Laboratory on Applied Optics, Changchun 130023, PR China
[c] Global Energy Interconnection Research Institute, Beijing 102211, PR China

ARTICLE INFO

Article history:
Received 31 July 2016
Received in revised form
24 October 2016
Accepted 9 November 2016
Available online 10 November 2016

Keywords:
Porous nanoparticles
MOFs
MIL-101(Cr)
Humidity sensor
Complex impedance

ABSTRACT

Metal organic framework MIL-101(Cr) nanoparticles were successfully HF- free synthesized via hydrothermal method and characterized by X-ray diffraction (XRD), scanning electron microscope (SEM) and Nitrogen adsorption-desorption technology. Then resistive humidity sensor was fabricated to investigate humidity sensing properties. The results indicate that the sensor shows high sensitivity and rapid response-recovery time. The impedance changes more than three orders of magnitude in the range of 33–95% RH at 100 Hz. The response time and recovery time are 17 s and 90 s respectively. Finally, the humidity sensing mechanism was discussed through complex impedance analysis. The results illustrate that porous MIL-101(Cr) nanoparticles have great potential to be used as humidity sensing materials.

1. Introduction

Humidity sensors play an important role in many aspects in our daily life, such as meteorology, agriculture, medicine, biology and so on. Due to various moisture requirements, humidity sensors are typically applied in industrial processes, environmental monitoring and equipment maintenance, which all need accurate humidity control. Thus a great deal of attention involving humidity sensors has been abstracted to improve the performance in recent years. Significant progress has been made based upon the selection of humidity materials especially [1,2]. The traditional ceramic materials with their good chemical properties and long lifetime are good candidates for humidity sensing layers [3–5]. However, the capacity of water adsorption usually needs to be improved by assistant calcination method [6]. Besides, although humidity sensors based on polymer materials are also immediate research focus [7–9], and have the advantage of diversity, their long-term stability remains a common problem [10].

In recent years, nano-porous crystalline materials reveal good performances in catalysis, photoelectron and gas sensing [11–14]. Metal Organic Frameworks (MOFs), as a new type of porous materials, start to attract people's great attentions [15–17]. Depending on the advantages of high specific surface area, high porosities and various framework structures, MOFs have shown wide applications in catalysis, gas separation and storage [18–20]. However, MOFs have been rarely considered as humidity materials because the skeletal structure may collapse in heavy moisture. Even if some MOFs were utilized, the humidity sensitivity was still low due to the limited specific surface areas [21,22]. In order to solve the problems, we present a typical Cr-base metal organic framework material MIL-101 for humidity sensor. The structure is a super tetrahedron which is made from Cr-trimers as four vertexes and the linkage of 1, 4-BDC anions as six edges [23]. The framework delimits two types of porous cages with inter free diameters of ~29 Å and ~34 Å. Obviously, the windows with different diameters can make water molecules accessible to the pores. The abundant hydrophilic active sites (chromium oxo-clusters) on the framework surface can also adsorb water molecules easily. What is more, MIL-101(Cr) possesses extremely high specific surface areas as well as water stability in comparison to other MOFs. Thus, MIL-101(Cr) can be

* Corresponding author. State Key Laboratory on Integrated Optoelectronics, College of Electronic Science & Engineering, Jilin University, Changchun 130012, PR China.
** Corresponding author.
E-mail addresses: guowb@jlu.edu.cn (W. Guo), ruansp1226@163.com (S. Ruan).

http://dx.doi.org/10.1016/j.jallcom.2016.11.129
0925-8388/

very good candidate for humidity sensor. In this study, we successfully fabricated the humidity sensor based on MIL-101(Cr) and investigated the humidity sensing properties. The sensor reveals high sensitivity and rapid response-recovery behavior in a wide humidity range.

2. Experimental

2.1. Preparation

Crude MIL-101(Cr) was HF-free synthesized by a hydrothermal method: 2.0 g $Cr(NO_3)_3 \cdot 9H_2O$ and 0.82 g Terephthalic acid were dissolved in 25 mL sodium acetate solution (0.05 mol/L) with stirring for 30 min. Then the mixed solution was transferred into a Teflon-lined autoclave, and heated at 220 °C for 8 h. After the reaction, green sample was collected. The sample was filtered off and washed by deionized water adequately. After drying at 60 °C for 8 h, crude product was obtained with a part of unreacted Terephthalic acid existing.

Next, the crude product was purified via subsequent processing [24]: 1.0 g crude product synthesized above was added to 50 mL ethanol and the mixture was transferred into a Teflon-lined autoclave at 100 °C for 20 h. After washing and drying, 0.5 g sample was mixed with 75 mL ammonium fluoride (30 mmol/L) with stirring completely, and then heating in water bath at 60 °C for 10 h. The sample was treated successively by filtration, washing and drying under vacuum, and pure MIL-101(Cr) was finally obtained.

2.2. Sensor fabrications

The prepared sample was grinded with deionized water in a weight ratio of 5: 1 to form a paste, and then covered on the ceramic substrates (6 mm × 3 mm × 0.5 mm) to form humidity sensing film. The substrates were fabricated by jetting Ag-Pd paste on ceramic plates through a metal-jetting system (MJ-10, Beijing Elite Tech Co., Ltd., China). One thing to note is that the paste needs to be located on the effective area of Ag-Pd interdigitated electrodes. After that, the film was dried at 80 °C for 8 h. Fig. 1 is the schematic of the humidity sensor structure.

2.3. Characterization

The composition of sample was detected by X-ray diffraction (XRD) on a Shimadzu XRD-6000 diffractometer with Cu Kα radiation (λ = 1.548 Å). The scanned range is from 2° to 18° with the rate of 0.5° min^{-1} and step size of 0.01°. The morphology of samples was characterized on scanning electron microscope (SEM) (JEOL JBM-7500F). Surface area of the samples was measured by a Nitrogen adsorption-desorption analyzer (Gemini VII 2390). We calculated specific surface area S_{BET} in the Brunauer-Emmett-Teller (BET) method. The humidity properties of samples were measured by a Precision Impedance Analyzer 6500B Serious of Wayne Kerr Electronics which provides the frequency ranging from 20 Hz to 100 kHz and AC voltage value 1 V. We choose five saturated salt solutions of $MgCl_2$, $Mg(NO_3)_2$, NaCl, KCl, and KNO_3 as humidity generation sources with their corresponding to the relative humidity values 33%, 54%, 75%, 85% and 95%, respectively [25].

3. Results and discussion

3.1. Structural and morphological characteristics

Fig. 2 shows the X-ray diffraction patterns of MIL-101(Cr). The characteristic peaks positions of the as-prepared samples (b) are consistent with those simulated (a) from crystal structure [24]. No impurity diffraction peaks are observed obviously.

To observe the morphology of MIL-101(Cr), we make a characterization by SEM. As is shown in Fig. 3, the nanoparticles present octahedral structure in shape, and the average particle diameter is about 150 nm.

For confirming the porous nature, we measure the Nitrogen adsorption and desorption of MIL-101(Cr) to calculate specific surface area S_{BET} by Brunauer-Emmett-Teller (BET) method. Fig. 4 shows the Nitrogen adsorption-desorption isotherm. It can be observed that the adsorption and desorption isotherms are not reversible with an obvious hysteresis loop at $P/P_0 > 0.6$. According to the IUPAC classification, the curve shape is a type-IV isotherm, which provides evidence for mesopore-size distribution. The specific surface area S_{BET} of MIL-101(Cr) is 2292.31 m^2/g and the pore volume is about 1.38 cm^3/g.

3.2. Humidity sensing properties

The impedances of MIL-101(Cr) in different RH conditions were measured with the frequencies from 20 Hz to 100 kHz. Fig. 5 shows the relationships between the impedance and RH at different frequencies. As we can see, the impedance decreases obviously with RH increase at low frequencies, while there is no obvious change at high frequencies because the polarization of adsorbed water molecules cannot be able to keep pace with the change of electric fields.

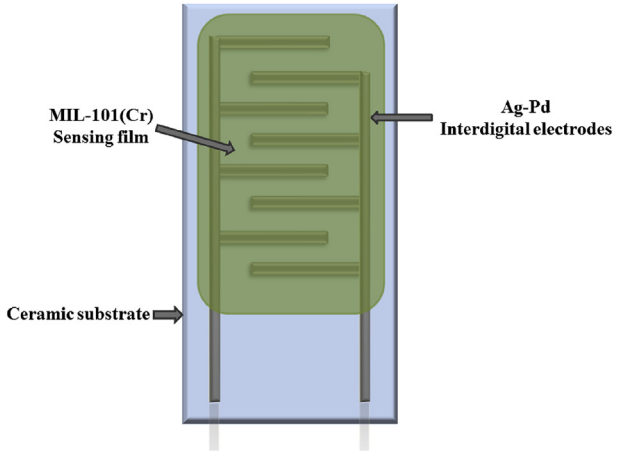

Fig. 1. Schematic of the resistive humidity sensor structure.

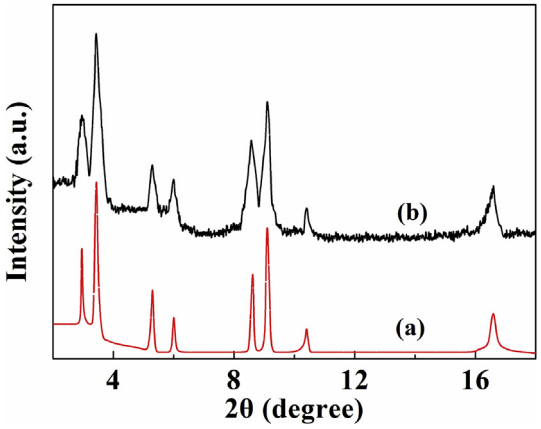

Fig. 2. X-ray diffraction patterns of MIL-101(Cr): the simulated from single crystal structure (a) and as-prepared samples (b).

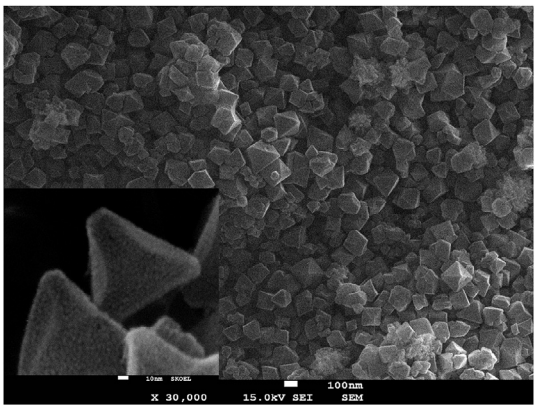

Fig. 3. SEM images of MIL-101(Cr).

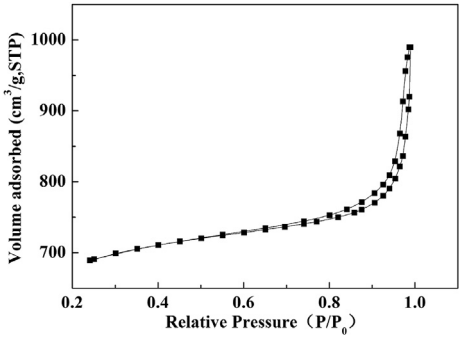

Fig. 4. Nitrogen adsorption-desorption isotherms of MIL-101(Cr).

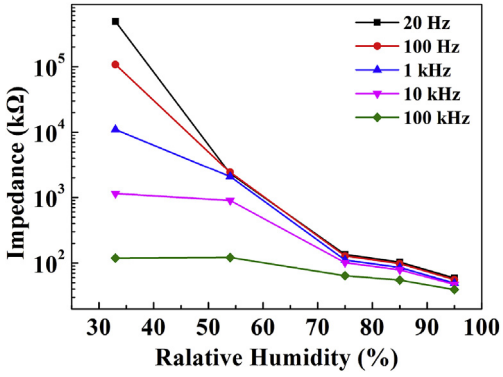

Fig. 5. Impedance-RH relationships of MIL-101(Cr) at different frequencies.

Thus, the best operating frequency is 100 Hz with high humidity sensitivity and good linearity. The impedance changes more than three orders of magnitudes from 107852 kΩ to 55.809 kΩ in the range of 33–95% RH. Therefore, the following tests were carried out at the frequency of 100 Hz.

The hysteresis characteristic of MIL-101(Cr) appears during the adsorption (from 33 to 95% RH) and desorption (from 95 to 33% RH) processes. Fig. 6 shows that the max humidity hysteresis is about 4% RH, indicating MIL-101(Cr) is a reliable and applicable material for humidity sensing.

The response and recovery time is also a most important factor for evaluating the performance of humidity sensors, which is shown in Fig. 7. The response time, which indicates the time needed by the sensor to achieve 90% of the whole impedance change (from 33 to 95% RH) during the adsorption process, is 17 s.

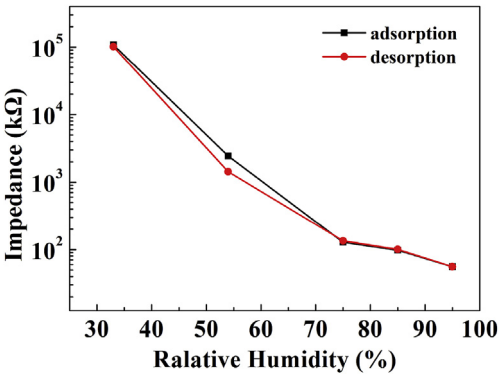

Fig. 6. Humidity hysteresis characteristic of MIL-101(Cr).

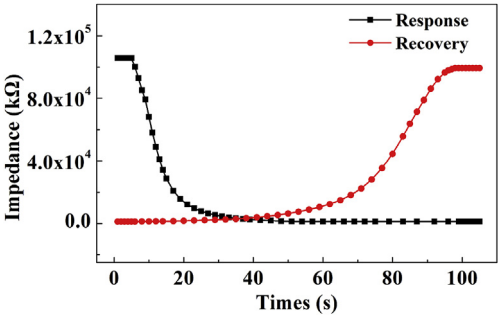

Fig. 7. Response and recovery behaviors of MIL-101(Cr).

Similarly, the recovery time, during the desorption process, is about 90 s. The rapid response-recovery behavior mainly relies on the porosity and high surface areas, which facilitate the transport of water molecules in the adsorption and desorption processes. The above results demonstrate that MIL-101(Cr) is suitable for humidity sensor.

The stability and reproducibility are significant parameters for the practicability of humidity sensors. The prepared humidity sensor was exposed to air environment, and the impedances were measured every 5 days under various RH. As is shown in Fig. 8a, no evident variation of impedances appears at fixed humidity in 30 days. Thus, the sensor exhibits good long-term stability. Fig. 8b is the humidity sensing curves of different devices based on as-prepared samples. There is high consistency among the curves of three sensors, confirming reproducibility of MIL-101(Cr) sensor.

In order to investigate the effects of interference on the sensor, we test the sensing response to other possible interference gases and volatile compounds. Fig. 9 presents the selectivity of MIL-101(Cr) sensor for humidity (33–95% RH) and other typical gases (1000 ppm) such as CO, NH_3, NO_2, methanal, ethanol and toluene with 42% RH. It is obvious that the sensor shows much higher response ($R_{33\%}/R_{95\%} = 1932$) to humidity than other tested interference gases, indicating the prominent selectivity for humidity. The above discussions show that the MIL-101(Cr) sensor is reliable for complicated environment in practical applications.

3.3. Sensing mechanism

In order to study the conduction mechanism of MIL-101(Cr) humidity sensor, we analyzed the complex impedance spectra in various RH with frequencies from 20 Hz to 100 kHz (Fig. 10).

In dry condition, the complex impedance spectra is a straight line (Fig. 10a), which represents the inherent resistance of the

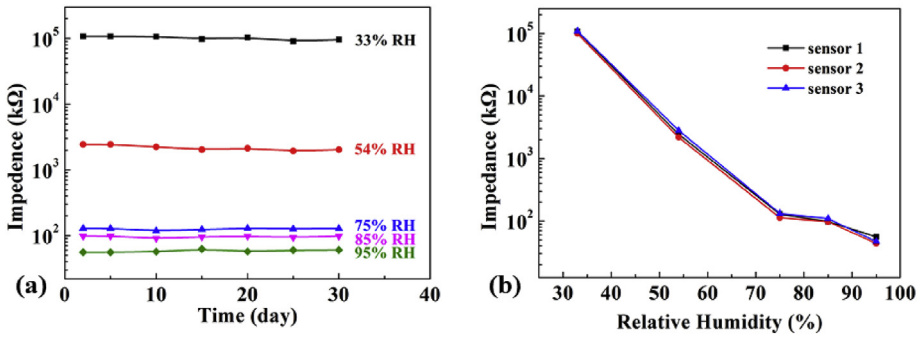

Fig. 8. (a) Stability of MIL-101(Cr) humidity sensor after exposing to air environment for 30 days, (b) Humidity sensing curves of different sensors based on MIL-101(Cr).

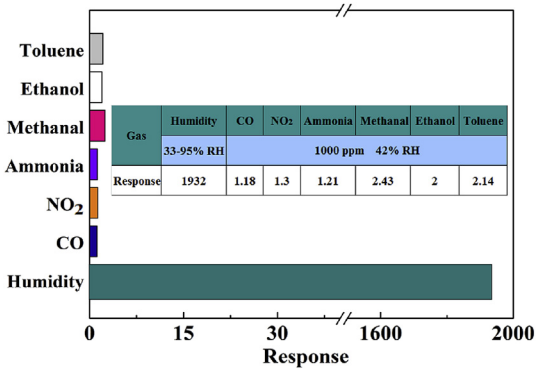

Fig. 9. Selectivity of MIL-101(Cr) humidity sensor for humidity (33–95% RH) and other possible interference gases and volatile compounds.

sensor and the impedance is extremely high. At 33% RH, a small number of water molecules are chemisorbed on the hydrophilic active sites (chromium oxo-clusters) and dissociated into H^+ and OH^- forming hydroxyl groups. Then these surface hydroxyl groups will be combined with water molecules by hydrogen bond, and protons can be transferred from hydroxyl groups to water molecules to come into hydronium ions (H_3O^+) [26]. These hydronium ions (H_3O^+) are the main charge carriers owing to the strong binding force between protons and water molecules [27]. H_3O^+ migrate directionally under the function of alternating electric field producing surface leakage current. We can conclude obviously that the whole complex impedance decreases and the complex impedance spectra changes from a straight line to an arc due to the surface leakage current (Fig. 10b). However, low RH only leads to a small quantity of hydronium ions (H_3O^+), so the impedance is still high. When RH increases to 54%, more water molecules adsorbed make the concentration of H_3O^+ higher, and then generate higher leakage current. So the impedance reduces markedly and the complex impedance spectra is gradually close to a semicircle curve (Fig. 10c). With the further increase of RH (75%), a large number of water molecules are chemisorbed on the whole surface of pores and form a liquid water layer. Subsequently, water molecules continue to adhere to the first liquid water layer by hydrogen bonds forming the second, third … …liquid water layer through physical adsorption, which eventually generate a network of continuous liquid water layers. At this time, the charges transfer mainly by Grotthuss chain reaction ($H_2O + H_3O^+ = H_3O^+ + H_2O$) in these continuous liquid water layers, that is H_3O^+ release H^+ to the adjacent water molecule forming another H_3O^+, which will next release another H^+ to other water molecule, and so on forth [28]. H^+ as the charge carrier induce space charge polarization resulting in a trend of straight line in the complex impedance spectra (Fig. 10d) when frequency is low. In the physisorbed layers of liquid water network, the charge transfer is dominant by H^+ between the adjacent water molecules. So the above process makes the conduction exploded and complex impedance declined. Since Grotthuss chain reaction occurs at low frequencies, the complex impedance spectra falls into two parts: straight line at low frequencies and semicircle curve at high frequencies. Furthermore, at high relative humidity (85%–95%), more and more water molecules are physically adsorbed on the surface that dramatically improves the conductive capacity of H^+ as well as the space charge polarization. Since the quality and radius of H_3O^+ are big, the directional migration of H_3O^+ cannot catch up with the alternating electric field when the frequency is very high, and the impact of H_3O^+ reduces. The space charge polarization of H^+ becomes predominant gradually with the increasing RH. So in the complex impedance spectra, the part of straight line becomes longer and the part of semicircle curve disappears slowly (Fig. 10e and f). In the whole process, the impedance declines obviously.

For further discussion about the sensing mechanism, the equivalent circuit could be modeled (Fig. 11) with complex impedance spectra fitting to measured data via computer software ZsimpWin. The results show that the equivalent circuit contains two series parts at low RH: one is resistance Rs; the other is the parallel connection of resistance R_1 and constant phase element CPE_1. The resistance Rs represents the portion of electrode which is irrelevant to RH. The arc and semicircle curves in complex impedance spectra are simulated by the parallel part of R_1 and CPE_1, which represents the interaction between sensing layer and water molecules. Therein, the resistance R_1 describes the bulk resistance of MIL-101(Cr) sensing layer and CPE_1 depicts the function of hydronium ions (H_3O^+) in MIL-101(Cr) layer. And at high RH, it could be concluded that the equivalent circuit contains two parts: one is resistance Rs; the other is the parallel connection of constant phase element CPE_1 and the series part concluding resistance R_1 and constant phase element CPE_2. The upturned lines at low frequencies in complex impedance spectra are signified by CPE_2, which depicts the impact of hydrogen ions (H^+) jumping between the water molecules in the physisorbed layers. As is shown in Fig. 8, all simulated data (Simu.) obtained by equivalent circuit are in accordance with the measured data (Msd.), which indicates that the process of mechanism analysis is appropriate for MIL-101(Cr) humidity sensor.

In conclusion, the main charge carrier is hydronium ion (H_3O^+) at low humidity. Moreover, with RH increasing, H^+ produced through Grotthuss chain reaction and hydronium ions (H_3O^+) are cooperative as main charge carriers. The impedance of MIL-101(Cr) humidity sensor decreases gradually in the whole process because of the growing number of carriers.

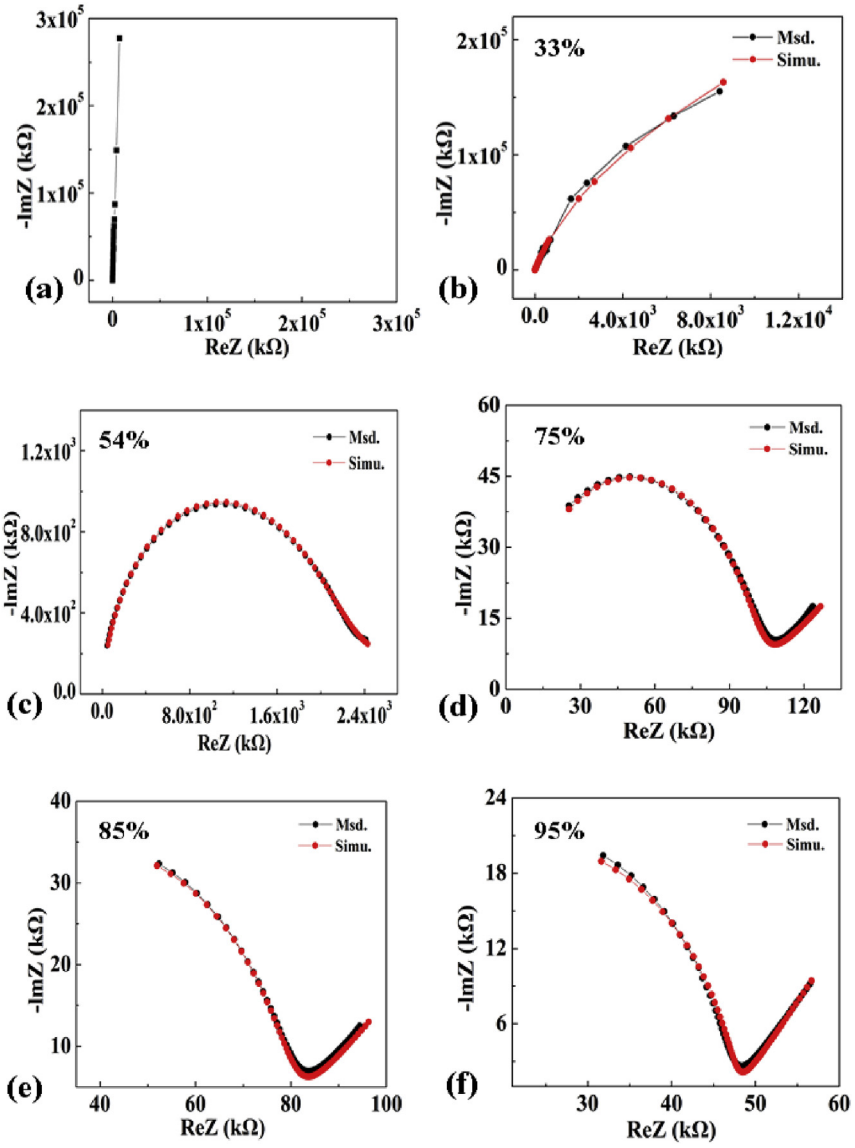

Fig. 10. Complex impedance properties of MIL-101(Cr) at various RH (0, 33, 54, 75, 85, 95%).

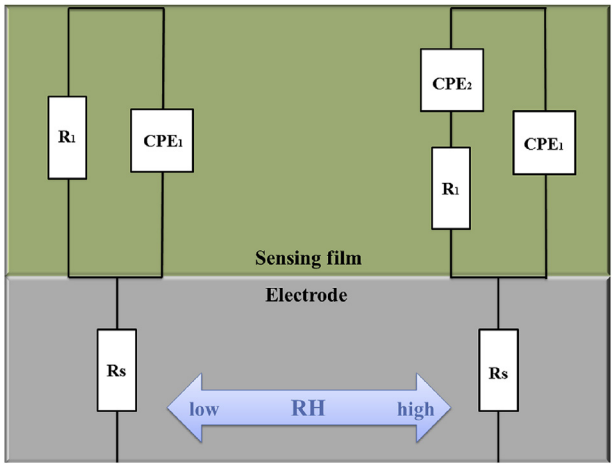

Fig. 11. Equivalent circuit model at different RH.

4. Conclusions

In summary, metal organic framework MIL-101(Cr) nanoparticles were successfully HF- free synthesized by hydrothermal method and purified. Then we fabricated the resistive humidity sensor and investigated the humidity sensing properties. The results show that the sensor reveals high sensitivity (impedance changes more than three orders of magnitudes in the range of 33–95% RH) as well as rapid response and recovery time (17 s and 90 s). These results illustrate that metal organic framework MIL-101(Cr) nanoparticles have extensive application prospect for RH detection.

Acknowledgements

This work was supported by the National Natural Science Foundation of China (Grant Nos. 11574110), Project of Statistic Analysis of Gas Sensitive Materials, Opened Fund of the State Key Laboratory on Applied Optics and Opened Fund of the State Key Laboratory on Integrated Optoelectronics (No. IOSKL2013KF10).

References

[1] R. Wang, X.W. Liu, Y. He, Q. Yuan, X.T. Li, G.Y. Lu, T. Zhang, Sens. Actuator B Chem. 145 (2010) 386–393.
[2] Y. Zhang, Y. Chen, Y. Zhang, X. Cheng, C. Feng, L. Chen, J. Zhou, S. Ruan, Sens. Actuator B Chem. 174 (2012) 485–489.
[3] Q. Kuang, C. Lao, Z. Wang, Z. Xie, L. Zheng, J. Am. Chem. Soc. 129 (2007) 6070–6071.
[4] H. Aoki, Y. Azuma, T. Asaka, M. Higuchi, K. Asaga, K. Katayama, Ceram. Int. 34 (2008) 819–822.
[5] A. Erol, S. Okur, B. Comba, O. Mermer, M.C. Arikan, Sens. Actuator B Chem. 145 (2010) 174–180.
[6] Y. Zhang, K. Yu, D. Jiang, Z. Zhu, H. Geng, L. Luo, Appl. Surf. Sci. 242 (2005) 212–217.
[7] K. Ocakoglu, S. Okur, Sens. Actuator B Chem. 151 (2010) 223–228.
[8] P.G. Su, W.C. Li, J.Y. Tseng, C.J. Ho, Sens. Actuator B Chem. 153 (2011) 29–36.
[9] S.K. Mahadeva, S. Yun, J. Kim, Sens. Actuator A Phys. 165 (2011) 194–199.
[10] H. Yoon, Nanomaterials 3 (2013) 524–549.
[11] G. Ferey, Chem. Soc. Rev. 37 (2008) 191–214.
[12] T.M. Suzuki, M. Yamamoto, K. Fukumoto, Y. Akimoto, K. Yano, J. Catal. 251 (2007) 249–257.
[13] F. Gao, S.P. Naik, Y. Sasaki, T. Okubo, Thin Solid Films 495 (2006) 68–72.
[14] Y. Zheng, X. Li, P.K. Dutta, Sensors 12 (2012) 5170–5194.
[15] M. Dan-Hardi, C. Serre, T. Frot, L. Rozes, G. Maurin, C. Sanchez, G. Ferey, J. Am. Chem. Soc. 131 (2009) 10857–10859.
[16] C. Zlotea, D. Phanon, M. Mazaj, D. Heurtaux, V. Guillerm, C. Serre, P. Horcajada, T. Devic, E. Magnier, F. Cuevas, G. Férey, P.L. Llewellyn, M. Latroche, Dalton Trans. 40 (2011) 4879–4881.
[17] Z. Zhang, Y. Zhao, Q. Gong, J. Li, Chem. Commun. 49 (2013) 653–661.
[18] Y. Fu, D. Sun, Y. Chen, R. Huang, Z. Ding, X. Fu, Z. Li, Angew. Chem. 124 (2012) 3420–3423.
[19] J. Li, R. Kuppler, H. Zhou, Chem. Soc. Rev. 38 (2009) 1477–1504.
[20] T. Segakweng, N.M. Musyoka, J. Ren, P. Crouse, Res. Chem. Intermed. 42 (2016) 4951–4961.
[21] J. Liu, F. Sun, F. Zhang, Z. Wang, R. Zhang, C. Wang, S. Qiu, J. Mater Chem. 21 (2011) 3775–3778.
[22] Y. Zhang, Y. Chen, Y. Zhang, H. Cong, B. Fu, S. Wen, S. Ruan, J. Nanopart. Res. 15 (2013), 2014.
[23] G. Férey, C. Mellot-Draznieks, C. Serre, F. Millange, J. Dutour, S. Surble, I. Margiolaki, Science 309 (2005) 2040–2042.
[24] D. Hong, Y. Kyu, C. Serre, G. Férey, J. Chang, Adv. Funct. Mater. 19 (2009) 1537–2155.
[25] L. Greenspan, J. Res. Natl. Bur. Stand. 81 (1977) 89–96.
[26] N. Yamazoe, Y. Shimizu, Sensors Actuators 10 (1986) 379–398.
[27] J.H. Anderson, G.A. Parks, J. Phys. Chem. 72 (1968) 3662–3668.
[28] N. Agmon, Chem. Phys. Lett. 244 (1995) 456–462.